Am J Cancer Res 2025;15(12):5231-5244
www.ajcr.us /ISSN:2156-6976/ajcr0169797

Original Article

IDH1 and ATRX mutations synergistically modulate cell proliferation and ferroptosis in glioblastoma cells

Siqi Liu[1], Xiangnan Xiao[2], Ang Li[2], Chao Ren[2], Bin Meng[2], Xiyu Huang[2], Xiao Wang[2], Lu Zhang[2], Mafei Xu[1,2]

[1]*Department of Pathophysiology, School of Basic Medical Sciences, Anhui Medical University, Hefei, Anhui, China;* [2]*Department of Cell Biology, School of Life Sciences, Anhui Medical University, Hefei, Anhui, China*

Received November 5, 2025; Accepted December 1, 2025; Epub December 15, 2025; Published December 30, 2025

Abstract: IDH1 and ATRX mutations frequently co-occur in several glioma subtypes, including secondary glioblastomas (GBMs), suggesting that these alterations may function cooperatively during tumor development. However, the molecular basis of their interaction remains poorly defined. In present study, we demonstrate that the *IDH1-R132H* mutation acts synergistically with ATRX loss to upregulate pro-proliferative genes while suppressing interferon (IFN) signaling. This coordinated effect supports the notion that the two mutations jointly promote tumor growth and attenuate anti-tumor immune responses. Notably, we also found that the combined *IDH1/ATRX* mutations increase GBM cell sensitivity to various forms of cell death, particularly ferroptosis. Mechanistically, the dual *IDH1/ATRX* alteration upregulates pro-ferroptotic genes (*HMOX1* and *ACSL4*) while downregulating anti-ferroptotic genes (*SLC7A11* and *GPX4*), thereby sensitizing GBM cells to ferroptosis induction. Together, our findings provide new biological insights into IDH1/ATRX-driven GBM pathogenesis and highlight ferroptosis as a potential therapeutic vulnerability in this aggressive tumor subtype.

Keywords: IDH1, ATRX, glioma, ferroptosis

Introduction

Gliomas are the most common primary tumors of the central nervous system, with roughly 300,000 new cases diagnosed worldwide each year [1]. According to the World Health Organization (WHO) classification, gliomas are divided into low-grade (I-II) and high-grade (III-IV) subtypes. Low-grade gliomas make up about 45% of diagnosis, most often diffuse astrocytomas (28%) and oligodendrogliomas (12%), whereas high-grade tumors account for the remaining cases, with glioblastoma (GBM) representing the most aggressive form and carrying a dismal five-year survival of only 5-10% [1, 2]. Among the genetic alterations seen in these tumors, mutations in *IDH1* - particularly the R132H variant - are the most prevalent [3, 4]. Notably, IDH1 mutations appear mainly in diffuse astrocytomas, oligodendrogliomas, and a subset of secondary glioblastomas, and their presence within a given tumor type is generally linked to better clinical outcomes, highlighting their importance in glioma biology [4-6].

The wild-type IDH1 protein forms a homodimer that converts isocitrate into α-ketoglutarate (α-KG). However, the R132H mutant pairs with the wild-type protein to form heterodimers that reduces α-KG to D-2-hydroxyglutarate (D-2HG), a metabolite that competes with α-KG and inhibits a wide range of α-KG-dependent dioxygenases, including Ten-eleven translocation (TET) methylcytosine dioxygenases and JmjC-domain-containing histone demethylases (JmjC-KDMs) [7-11]. Their inhibition disrupts normal epigenetic regulation, leading to genome-wide DNA and histone methylation changes. One well-known consequence is the glioma CpG island methylator phenotype (G-CIMP), which alters the expression of pathways such as TGF-β and VEGF signaling [12-14]. In addition, hypermethylation-mediated silencing of *cGAS*, *STING*, and various transposable elements weakens type I interfer-

https://doi.org/10.62347/OXRW2934

on responses and contributes to immune evasion [15].

IDH1-mutant tumors frequently harbor loss-of-function mutations in *ATRX*, a chromatin remodeler responsible for H3.3 deposition and heterochromatin maintenance [16-18]. ATRX loss destabilizes telomeric chromatin and promotes the alternative lengthening of telomeres (ALT) pathway [19]. Studies have shown that IDH1 mutations and ATRX loss can reinforce one another - for example, by reducing the expression of DNA-repair factors such as RAP1 and XRCC1, which further supports the ALT phenotype [20]. Interestingly, the two alterations influence innate immunity in opposite ways: ATRX loss can elevate the expression of transposable elements and activate type I interferon pathways, whereas mutant IDH1 suppresses these same responses [15, 21]. How these seemingly conflicting effects shape tumor evolution and treatment sensitivity is still not fully understood.

Ferroptosis is an iron-dependent form of regulated cell death characterized by excessive accumulation of lipid peroxides and subsequent plasma membrane rupture. It is typically driven by oxidative stress and elevated reactive oxygen species, conditions common in metabolically active cancer cells [22, 23]. Cellular defense against ferroptosis primarily depends on glutathione peroxidase 4 (GPX4), which detoxifies lipid hydroperoxides in glutathione-dependent manner [24, 25]. Blocking glutathione synthesis with compounds such as Erastin, or inhibiting GPX4 directly with RSL3, can therefore trigger ferroptosis [24, 26]. Given their metabolic demands, glioma cells may be especially vulnerable to this process. Nevertheless, the mechanisms regulating ferroptosis in glioma remain poorly understood.

In this study, we established isogenic GBM cell lines harboring the IDH1-R132H mutation, ATRX knockout, or both. We demonstrate that the dual mutation enhances the expression of cell cycle - related proteins and promotes cellular proliferation. Notably, cells harboring both mutations display increased susceptibility to ferroptosis inducers due to dysregulation of genes involved in lipid and iron metabolism. These findings suggest that therapeutic induction of ferroptosis may represent a viable strategy for treating gliomas with concurrent IDH1 and ATRX mutations.

Results

IDH1 and ATRX double mutation is associated with gene signatures of cell proliferation and immunosuppression in GBM

We first examined the status of *IDH1* and *ATRX* mutations across different glioma subtypes. As shown in **Figure 1A** and **1B**, *IDH1* mutations occurred at high frequencies in anaplastic oligodendroglioma, oligodendroglioma, diffuse astrocytoma, and anaplastic astrocytoma, whereas their frequencies were lower in glioblastoma (GBM) and diffuse glioma. Notably, in diffuse astrocytoma, anaplastic astrocytoma and GBM, *IDH1* mutations were frequently accompanied by *ATRX* mutations. Given the generally poor prognosis of GBM, we further compared patient outcomes based on different mutation profiles. We found that *IDH1* mutation, either alone or co-occurring with *ATRX* mutation, was associated with improved prognosis, consistent with previous reports (**Figure 1C**). However, no significant difference was observed between the *IDH1*-only and *IDH1/ATRX* double-mutant groups, possibly due to the limited sample size.

To investigate whether the combined *IDH1/ATRX* mutation differs functionally from *IDH1* mutation alone during glioma progression, we carried out Gene Set Enrichment Analysis (GSEA). Relative to samples without either alteration, the *IDH1*-mutant group showed enrichment of programs associated to E2F targets, MYC targets, and DNA repair, while pathways associated with interferon gamma and inflammatory response were reduced (**Figure 1D**). These changes are consistent with earlier work reporting that the *IDH1* mutation tends to enhance proliferation and dampen immune activation. When both *IDH1* and *ATRX* were altered, the enrichment patterns became even more pronounced: E2F targets and G2M checkpoint pathway were further upregulated, whereas interferon gamma and inflammatory response pathways were further suppressed (**Figure 1E**). This pattern suggests that loss of ATRX may reinforce the growth-promoting and immune-suppressive effects initiated by mutant *IDH1*, which could help explain why

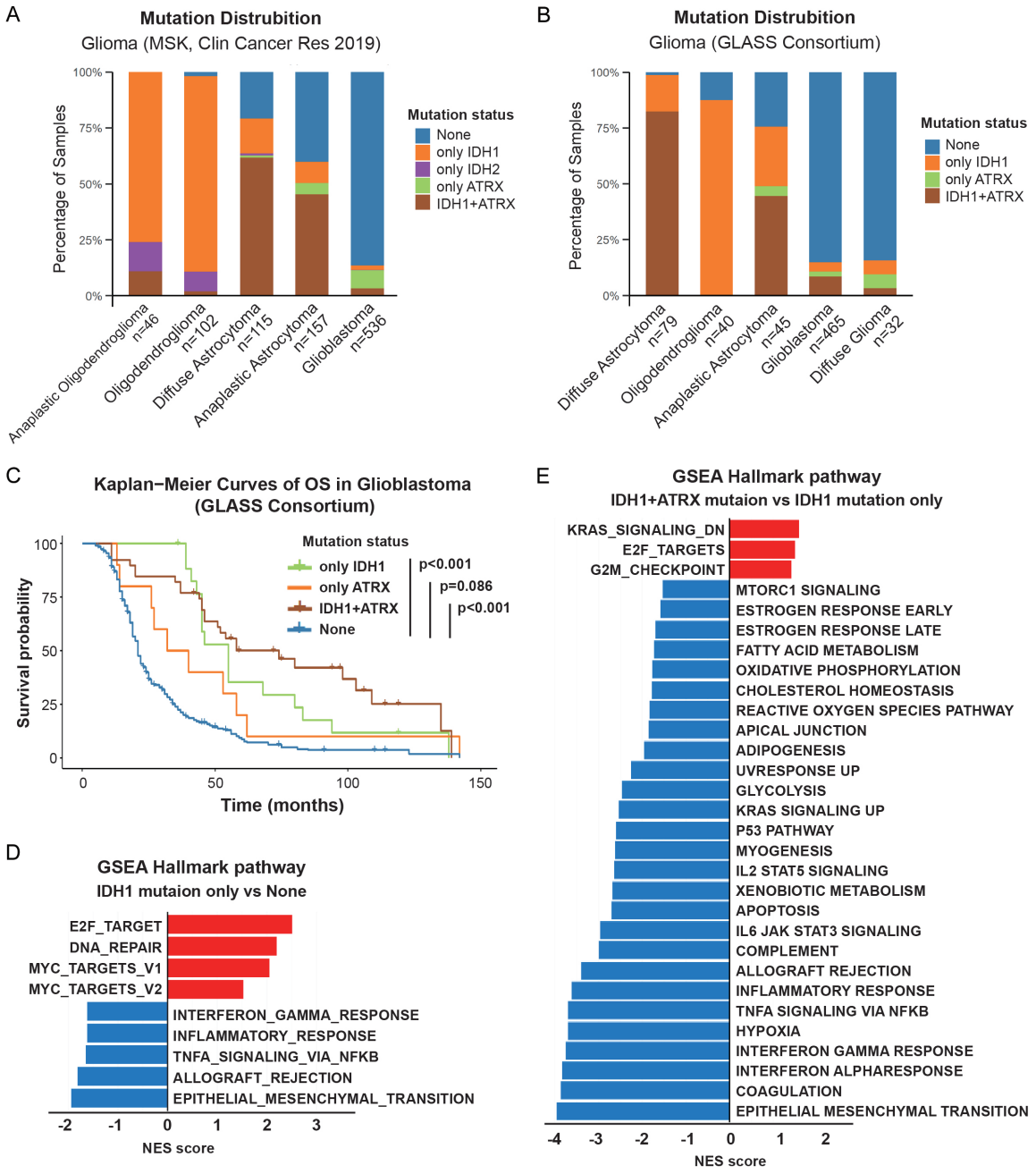

Figure 1. The clinical relevance of IDH1 and ATRX mutation in Glioma. (A, B) Distribution of *IDH1/2* and *ATRX* mutations across glioma subtypes in the MSK 2019 dataset (A) and GLASS Consortium dataset (B). (C) *IDH1* and/or *ATRX* mutations are associated with prolonged overall survival. (D, E) GSEA analysis of pathways associated with the mutation status as indicated: *IDH1* mutation only vs None of *IDH1* or *ATRX* mutation (D); *IDH1/ATRX* double mutation vs *IDH1* mutation only (E).

these mutations frequently appear together in gliomas.

IDH1-R132H and ATRX loss jointly influence proliferation and cell death in GBM cells

To probe these interactions experimentally, we generated T98G cell lines with *IDH1-R132H* overexpression, *ATRX* knockout, or both alterations (**Figure 2A**, **2B**), and referred them as mIDH1^{OE}, ATRX^{KO}, and mIDH1^{OE}+ATRX^{KO}, respectively. As expected, mIDH1^{OE} cells accumulated 2-hydroxyglutarate (2-HG), confirming the altered enzymatic activity of the mutant protein (**Figure 2C**, **2D**). Through CCK-8 and colony formation assays, we found that mIDH1^{OE} enhan-

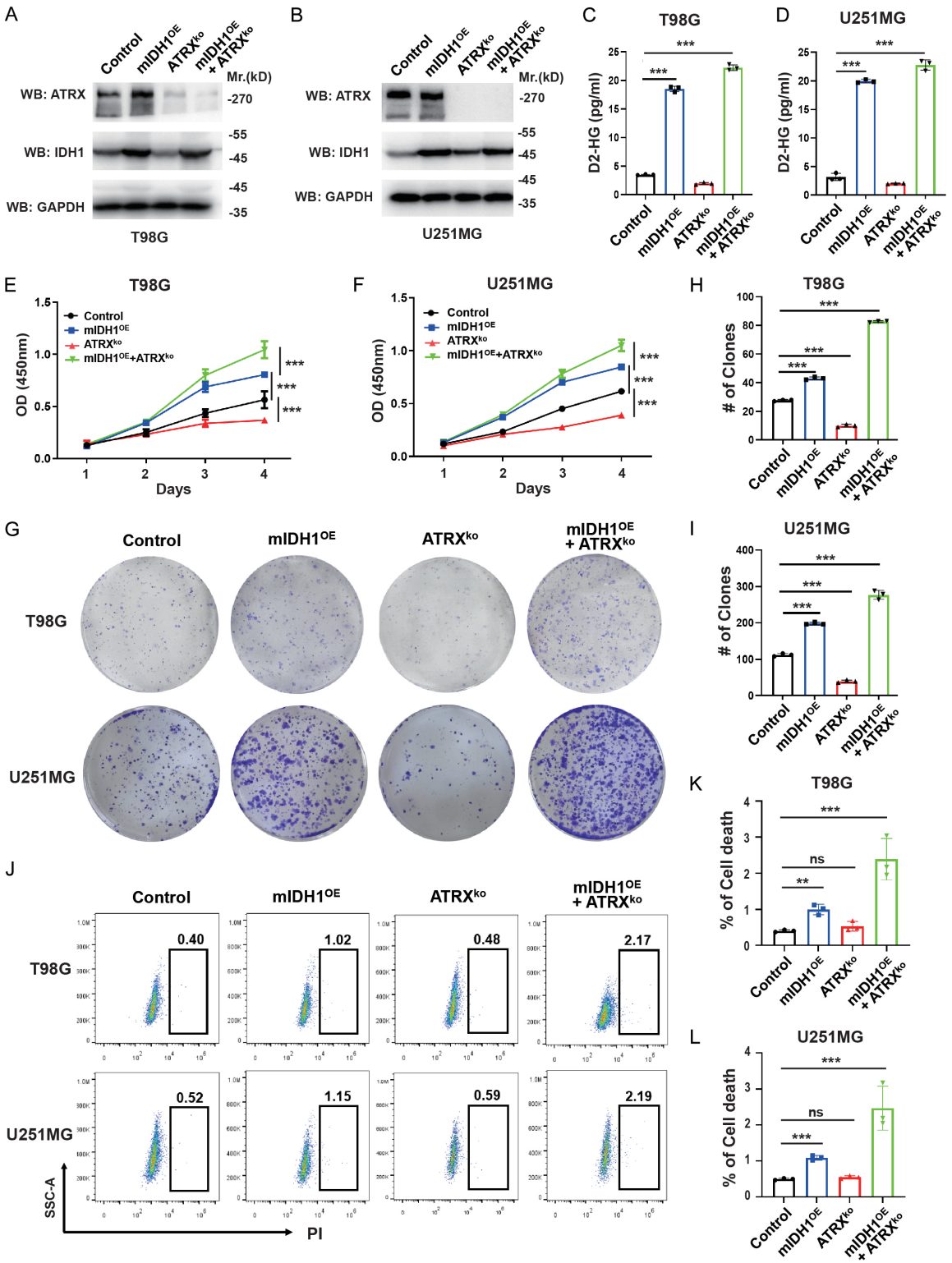

Figure 2. Synthetic effects of IDH1 and ATRX mutations on GBM cell proliferation and survival. (A, B) Western blotting analysis showing *ATRX* knockout efficiency and *IDH1-R132H* overexpression in T98G (A) and U251MG (B) cells. (C, D) Quantification of D2-HG levels in T98G (C) and U251 (D) cells with *IDH1-R132H* overexpression and/or *ATRX* knockout. (E, F) Cell proliferation accessed by CCK-8 assay. (G-I) Representative image (G) and quantification (H, I) of colony formation assays. (J-L) Representative FACS plots (J) and Quantification (K, L) of PI staining in different cell groups. Data are presented as mean ± SEM, and statistical significance was determined using one-way ANOVA followed by multiple comparisons testing. *P < 0.05; **P < 0.01; ***P < 0.001; ns, nonsignificant.

ced cell proliferation, whereas $ATRX^{KO}$ had the opposite effect. Interestingly, $mIDH1^{OE}$+$ATRX^{KO}$ cells displayed even greater proliferation and more colony formation than $mIDH1^{OE}$ alone (**Figure 2E-I**), indicating that ATRX loss can intensify the pro-proliferative effect of the IDH1 mutation.

Subsequently, we performed Propidium Iodide (PI) staining following flow cytometry analysis to detect cell death. Surprisingly, $mIDH1^{OE}$ cells exhibited higher baseline cell death than controls, and this effect was further increased in the double-mutant cells (**Figure 2J-L**). These observations indicate that mutant IDH1 promotes both cell proliferation and death, and that ATRX loss magnifies both processes.

IDH1-R132H and ATRX loss coordinate to suppress interferon signaling and upregulate proliferation-associated genes

Next, we performed RNA sequencing to characterize the transcriptional programs associated with these phenotypes. Using $|\log_2 FC| \geq 1$ and $P \leq 0.05$ as thresholds, $mIDH1^{OE}$ cells exhibited 1,062 upregulated and 1,025 downregulated genes compared with controls (**Figure 3A**). In $mIDH1^{OE}$+$ATRX^{KO}$ group, 1,116 genes were upregulated and 909 were downregulated relative to control, with an additional 463 upregulated and 225 downregulated when compared with $mIDH1^{OE}$ group (**Figure 3C**, **3E**). Consistent with clinical dataset analyses, GSEA demonstrated that *IDH1-R132H* suppressed interferon gamma/alpha and inflammatory response pathways, with *ATRX* loss causing further suppression (**Figure 3B**, **3D**, **3F**).

Although GSEA did not reveal significant enrichment of E2F targets or G2M checkpoint pathways, further examination of key genes showed synergistic regulation. For instance, *MYC* expression remained unchanged in single mutants but was significantly upregulated in the double mutant (**Figure 3G**). Similarly, *E2F2* was upregulated by *IDH1-R132H* alone and further elevated with *ATRX* loss (**Figure 3G**). These results were validated via qPCR in both T98G and U251MG cells (**Figure 3H** and **3I**). Collectively, these findings indicate that *ATRX* loss cooperates with *IDH1-R132H* to upregulate pro-proliferative genes, which may explain their co-occurrence in GBM.

IDH1-R132H and ATRX loss synergistically sensitize GBM cells to ferroptosis

Since the GSEA results did not point to a specific pathway responsible for the increased cell death, we assessed how the cells responded to several well-established death-inducing agents: Staurosporine (apoptosis), Rapamycin (autophagy), Nigericin (pyroptosis), and Erastin (ferroptosis) [26-29]. As shown in **Figure 4A** and **4B**, $mIDH1^{OE}$ cells showed a noticeable rise in death, $ATRX^{KO}$ cells displayed little change, and the double-mutant cells exhibited the strongest response. Among these treatments, Erastin consistently caused the highest increase of cell death in $mIDH1^{OE}$+$ATRX^{KO}$ cells, leading us to investigate ferroptosis in greater detail.

CCK-8 assays further demonstrated that $mIDH1^{OE}$+$ATRX^{KO}$ cells were more sensitive to ferroptosis inducers, as reflected by markedly reduced IC_{50} values for both Erastin and RSL3 (**Figure 4C-F**). In parallel, BODIPY-C11 staining showed increased lipid peroxidation in the double-mutant cells under basal conditions as well as after ferroptosis induction (**Figure 4G**, **4H**). These results support the conclusion that the combination of IDH1-R132H and ATRX loss makes GBM cells more vulnerable to ferroptosis.

RNA-seq analysis indicated that IDH1-R132H lowers the levels of the anti-ferroptotic genes GPX4 and SLC7A11, while elevating HMOX1 and ACSL4, which participate in iron metabolism and polyunsaturated fatty-acid synthesis, respectively (**Figure 5A**, **5B**). These expression trends were validated by qPCR and western blot in T98G and U251MG cells (**Figure 5C-E**). ATRX loss further reduced GPX4 and increased HMOX1 expression, consistent with the heightened ferroptotic sensitivity of double-mutant cells (**Figure 5C-E**). Together, these findings suggest that IDH1-R132H and ATRX loss cooperatively enhance ferroptosis sensitivity in GBM cells by promoting pro-ferroptotic gene expression and dampening key protective pathways.

Discussion

Although the co-occurrence of *IDH1* and *ATRX* mutations in glioma has long been recognized, the mechanisms underlying their synergistic function in tumor development remain poorly

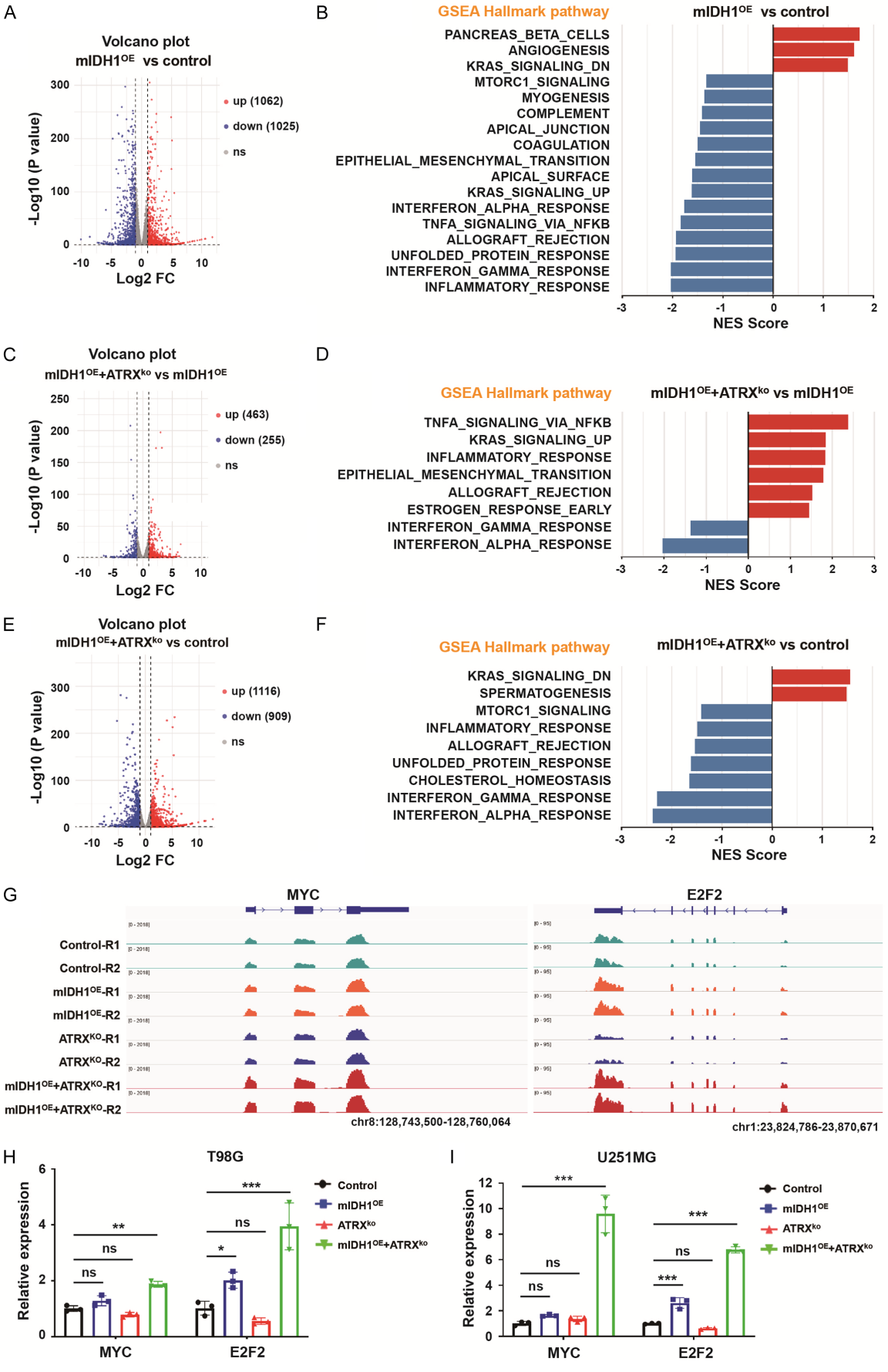
A
Volcano plot
mIDH1OE vs control
up (1062)
down (1025)
ns
-Log10 (P value)
Log2 FC
B
GSEA Hallmark pathway
mIDH1OE vs control
PANCREAS_BETA_CELLS
ANGIOGENESIS
KRAS_SIGNALING_DN
MTORC1_SIGNALING
MYOGENESIS
COMPLEMENT
APICAL_JUNCTION
COAGULATION
EPITHELIAL_MESENCHYMAL_TRANSITION
APICAL_SURFACE
KRAS_SIGNALING_UP
INTERFERON_ALPHA_RESPONSE
TNFA_SIGNALING_VIA_NFKB
ALLOGRAFT_REJECTION
UNFOLDED_PROTEIN_RESPONSE
INTERFERON_GAMMA_RESPONSE
INFLAMMATORY_RESPONSE
NES Score
C
Volcano plot
mIDH1OE+ATRXko vs mIDH1OE
up (463)
down (255)
ns
-Log10 (P value)
Log2 FC
D
GSEA Hallmark pathway
mIDH1OE+ATRXko vs mIDH1OE
TNFA_SIGNALING_VIA_NFKB
KRAS_SIGNALING_UP
INFLAMMATORY_RESPONSE
EPITHELIAL_MESENCHYMAL_TRANSITION
ALLOGRAFT_REJECTION
ESTROGEN_RESPONSE_EARLY
INTERFERON_GAMMA_RESPONSE
INTERFERON_ALPHA_RESPONSE
NES Score
E
Volcano plot
mIDH1OE+ATRXko vs control
up (1116)
down (909)
ns
-Log10 (P value)
Log2 FC
F
GSEA Hallmark pathway
mIDH1OE+ATRXko vs control
KRAS_SIGNALING_DN
SPERMATOGENESIS
MTORC1_SIGNALING
INFLAMMATORY_RESPONSE
ALLOGRAFT_REJECTION
UNFOLDED_PROTEIN_RESPONSE
CHOLESTEROL_HOMEOSTASIS
INTERFERON_GAMMA_RESPONSE
INTERFERON_ALPHA_RESPONSE
NES Score
G
MYC
E2F2
Control-R1
Control-R2
mIDH1OE-R1
mIDH1OE-R2
ATRXKO-R1
ATRXKO-R2
mIDH1OE+ATRXKO-R1
mIDH1OE+ATRXKO-R2
chr8:128,743,500-128,760,064
chr1:23,824,786-23,870,671
H
T98G
Relative expression
Control
mIDH1OE
ATRXko
mIDH1OE+ATRXko
MYC
E2F2
I
U251MG
Relative expression
Control
mIDH1OE
ATRXko
mIDH1OE+ATRXko
MYC
E2F2

Figure 3. IDH1-R132H and ATRX depletion coordinately suppress IFN signaling and upregulate proliferation-associated genes. (A-F) Volcano plot showing transcriptomic differences among T98G groups (A/C/E), and GSEA plots illustrating enriched pathways associated with *IDH1-R132H* overexpression and *ATRX* knockout (B/D/F). (G) RNA-seq tracks showing expression of *MYC* and *E2F2* genes in T98G cells. (H, I) qPCR validation demonstrating that *IDH1-R132H* overexpression and *ATRX* knockout increase *MYC* and *E2F2* expression in T98G (H) and U251MG (I) cells. Data are presented as mean ± SEM, and statistical significance was determined by one-way ANOVA followed by multiple comparisons testing. *P < 0.05; **P < 0.01; ***P < 0.001; ns, nonsignificant.

understood. In this study, we demonstrate that the *IDH1-R132H* mutation and *ATRX* loss coordinate to promote GBM cell proliferation and suppresses anti-tumor immunity pathways. Moreover, the dual mutation leads to dysregulation of ferroptosis-associated genes, sensitizing GBM cells to ferroptosis inducers. Collectively, our findings reveal a novel mechanism through which *IDH1* and *ATRX* mutations drive GBM progression and highlight a potential therapeutic vulnerability.

IDH1 mutation is recognized as early event during glioma development, leading to G-CIMP formation and altered histone methylation patterns. These epigenetic changes activate cell proliferation-associated genes (e.g., *PDGF*, *CCND1*) while suppressing apoptosis-related genes (e.g., *BAX*, *CASP3*), thereby initiating gliomagenesis [12, 13, 30]. However, *IDH1* mutation alone is insufficient to induce glioma formation in animal models. Beatrice Philip et al. reported that co-expression of mutant *IDH1* with *PDGF1* overexpression and loss of *ATRX* and *PTEN* induces glioma *in vivo*, suggesting that *IDH1* mutation cooperates with other genomic alterations to promote tumor progression [31]. Furthermore, *IDH1* mutation can cause hypermethylation of the *MGMT* promoter, impairing its DNA repair function and increasing glioma sensitivity to temozolomide (TMZ) [32]. Our study shows that *IDH1* and *ATRX* mutations synergistically upregulate proliferation-associated genes such as *MYC* and *E2F2*, providing new mechanistic insight into their cooperative role in gliomagenesis.

Recent studies have revealed the critical roles of IDH1 and ATRX alterations in modulating tumor immunity. *IDH1* mutation suppressed type I interferon-mediated anti-tumor immune responses through DNA hypermethylation, which silences endogenous retroviral elements and reduces the expression of *STING*, *cGAS*, and *IFNB1* [15]. Consistently, IDH1-mutant GBMs typically display a T-cell-excluded phenotype, and pharmacologic inhibition of IDH1-R132H can restore dsDNA-driven immune activation [15, 33]. On the other hand, ATRX loss has been reported to upregulate immune checkpoint molecules PD-L1 and PD-L2 and to alter cytokine profiles, thereby reinforcing the immunosuppressive microenvironment of IDH1-mutant gliomas [34]. In line with these findings, our analyses of patient datasets and engineered cell models show that interferon signaling is suppressed by IDH1 mutation and further diminished upon ATRX loss, highlighting a cooperative role in shaping an immune-suppression phenotype.

Unexpectedly, we also observed that GBM cells with dual mutations are more sensitive to ferroptosis, accompanied by dysregulation of GPX4, SLC7A11, HMOX1, and ACSL4. IDH1 mutation downregulates SLC7A11 and GPX4, thereby impairing a central anti-ferroptotic defense: SLC7A11 encodes a subunit of system Xc^-, which mediates cystine uptake and supports glutathione synthesis, whereas GPX4 detoxifies lipid hydroperoxides in a glutathione-dependent manner [24, 26]. Concurrently, IDH1 mutation upregulates HMOX1 and ACSL4, with HMOX1 promoting heme degradation and iron release [35], and ACSL4 enriching membrane phospholipids with polyunsaturated fatty acids [36], both of which enhance ferroptotic susceptibility. Moreover, ATRX loss amplified these effects by further suppressing GPX4 and increasing HMOX1 levels. To our knowledge, this is the first study to link the combined IDH1/ATRX mutation to ferroptosis susceptibility in GBM, suggesting that ferroptosis-based therapeutic strategies may be particularly effective for this molecular subtype.

In summary, through analyses of patient datasets and validation in cell-based models, we reveal that the *IDH1/ATRX* double mutation promotes GBM cell proliferation while simultaneously increasing susceptibility to ferroptosis. By elucidating the underlying transcriptional mechanisms, our study provides new biological insight into *IDH1/ATRX*-driven gliomagenesis and identifies ferroptosis as a promising therapeutic target for this aggressive tumor subtype.

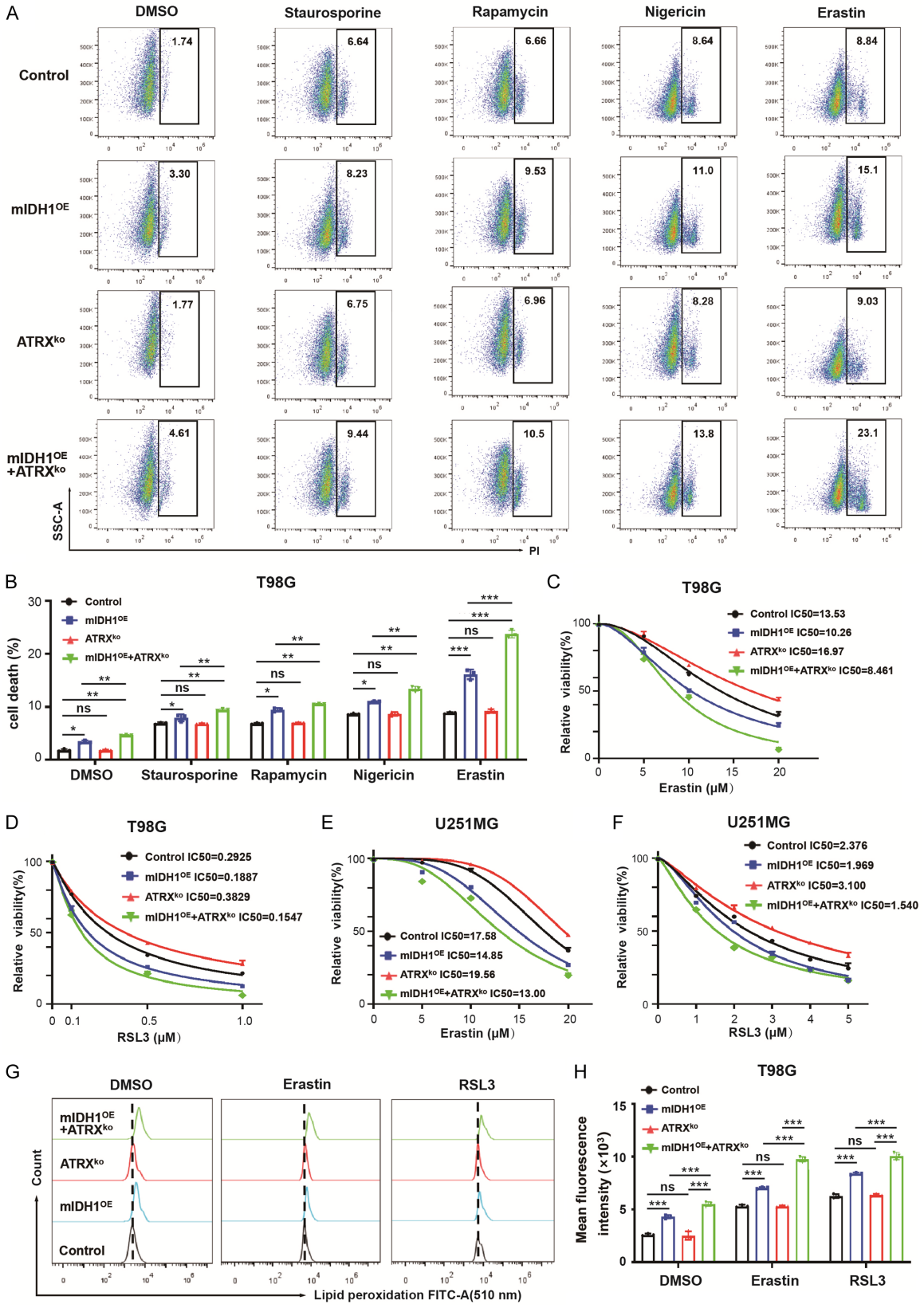

Figure 4. IDH1-R132H and ATRX depletion synergistically sensitized GBM cells to ferroptosis induction. (A, B) Representative FACS plots (A) and quantification (B) of PI staining in T98G cells treated with different death-inducing agents. (C-F) *IDH1-R132H* overexpression and *ATRX* knockout reduce the IC_{50} values of RSL3 and Erastin in T98G

(C, D) and U251MG (E, F) cells. (G, H) Representative FACS plots (G) and quantification (H) of lipid peroxidation in T98G cells treated with Erastin or RSL3. Data are presented as mean ± SEM, and statistical significance was determined by one-way ANOVA followed by multiple comparisons testing. *P < 0.05; **P < 0.01; ***P < 0.001; ns, nonsignificant.

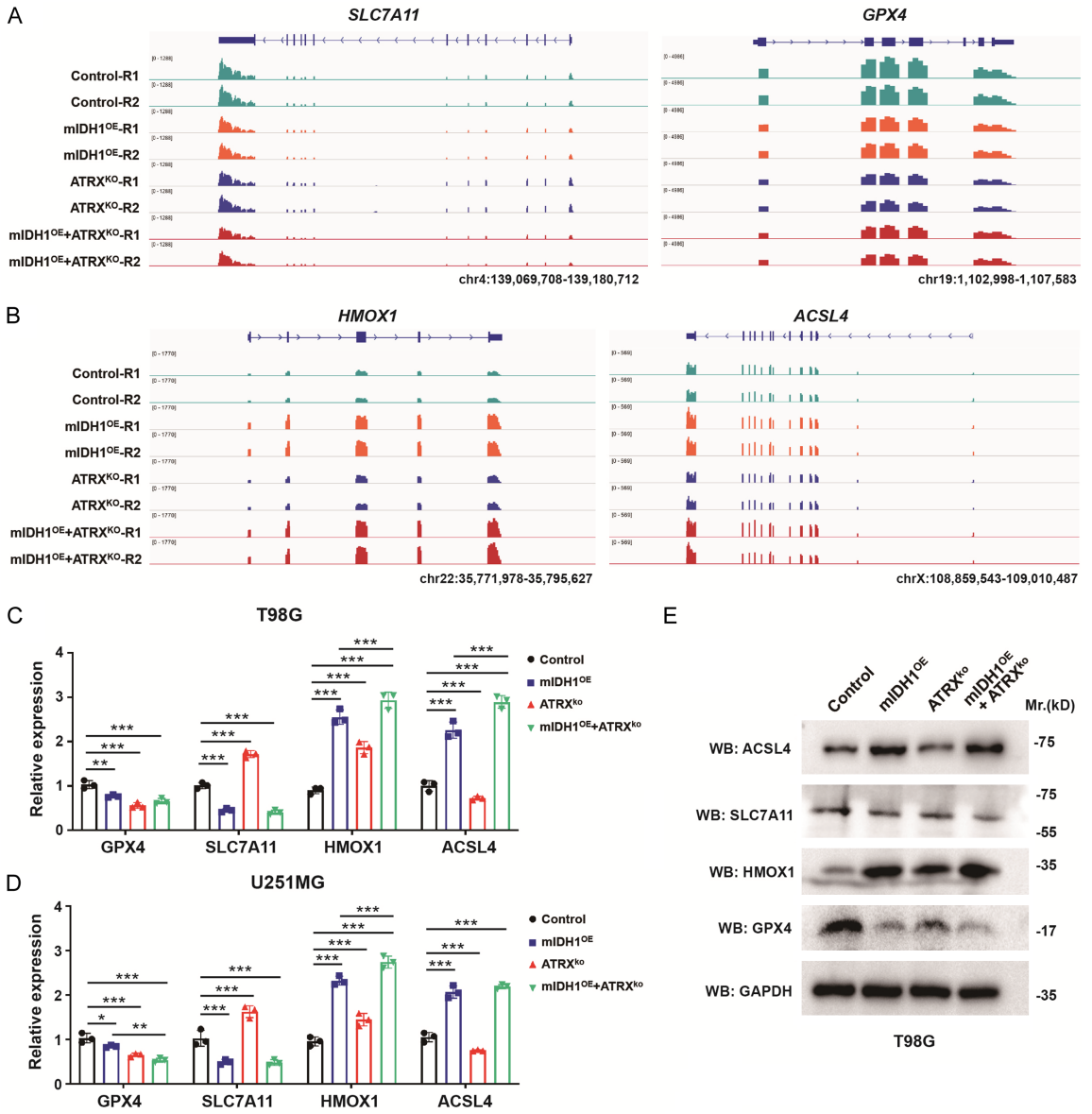

Figure 5. IDH1-R132H and ATRX depletion cooperatively regulate ferroptosis-associated gene expression. (A, B) RNA-seq tracks showing expression of anti-ferroptotic genes (*SLC7A11*, *GPX4*) (A) and pro-ferroptotic genes (*HMOX1*, *ACSL4*) (B) in T98G cells. (C-E) qPCR (C, D) and western blot (E) confirming that *IDH1-R132H* overexpression and *ATRX* knockout downregulate *SLC7A11* and *GPX4*, while upregulating *HOMX1* and *ACSL4* in T98G and U251MG cells. Data are presented as mean ± SEM, and statistical significance was determined by one-way ANOVA followed by multiple comparisons testing. *P < 0.05; **P < 0.01; ***P < 0.001; ns, nonsignificant.

Materials and methods

Please see the Supplemental Methods for information on the expression plasmids, sgRNAs, siRNAs, primers and antibodies (Tables S1, S2, S3, S4, S5, S6).

Public dataset analysis

Clinical data were obtained from MSK and GLASS Consortium datasets using cBioPortal [37, 38]. The mutation status analysis was performed with cBioPortal database web tools.

Survival analysis was estimated by the Kaplan-Meier method and analyzed by the log-rank test. Gene set enrichment analysis was performed with GSEA 4.1.0.

Cell culture

Human prostate cancer cell lines T98G, U251MG were purchased from American Type Culture Collection (ATCC). T98G was cultured in Minimum Essential Medium (KeyGEN Bio TECH) supplemented with 10% fetal bovine serum. U251MG was cultured in Dulbecco's Modified Eagle Medium (Procell system) supplemented with 10% fetal bovine serum. All cell lines were regularly tested to confirm that they were free of mycoplasma contamination.

Plasmid construction and Lentivirus infection

For generating pLVX-IDH1^{R132H} plasmid, the CDS of homo sapiens IDH1^{R132H} was cloned into the pLVX-M-puro vector. SgRNA expression plasmids targeting the human ATRX gene were designed by CRISPick. Oligos were synthesized by Tsingke Biotechnology Co., Ltd. Paired oligos were annealed and then inserted into the BsmBI site of the LentiGuide-puro vector.

Lentivirus were generated by co-transfection of expressing plasmid, pCMV-deltaR8.9 and pLP-VSVG into 293T cells. The infectious supernatants were harvested 72 hours after transfection, filtered through a 0.45-μM filter, mixed with polybrene (5 μg/ml), then added to T98G and U251MG cells. After 48 hours, the positive cells were selected with a final concentration of 1 or 2 μg/ml puromycin (Meilunbio; MA0318), 2 or 10 μg/ml blasticidin (Meilunbio; MB2506-1), or 400 or 800 μg/ml Geneticin (Meilunbio; MA0321). The overexpression and the inhibition efficiency were determined by Western blotting.

RT-qPCR

Total RNA was extracted by using FastPure Cell/Tissue Total RNA Isolation Kit (Vazyme). cDNA was prepared using a High-Capacity cDNA Reverse Transcription kit (BestEnzymes, 11201ES03). Quantitative PCR reactions were prepared with SYBR Green Master Mix (Yeasen Biotechnology (Shanghai) Co., Ltd.), and performed on a Celemetor96 Real-Time PCR System (Yeasen Biotechnology (Shanghai) Co., Ltd.). Relative transcript levels were calculated using the $^{\Delta\Delta}$CT method and normalized to β-actin.

Western blotting

Cells were homogenized and lysed using RIPA lysis buffer containing protease inhibitor cocktails (Thermo Scientific). Protein was quantified using the BCA assay, and an equal amount of protein for each lysate (50 ug) was resolved by 4-12% gradient SDS-PAGE followed by transfer onto nitrocellulose membranes. Membranes were blocked with 5% milk for 1 hour in tris buffered saline and probed with primary antibodies overnight at 4°C, followed by washing and probed with secondary antibody for 1 hour at room temperature. Pierce™ ECL Western Blotting Substrate (Thermo Fisher Scientific, PI32106) was used to develop chemiluminescent signals that were measured on an IVIS Lumina imager.

Enzyme-linked immunosorbent assay (ELISA)

The levels of D-2HG were analyzed by ELISA kits (Meimian, China, 51885H1). Briefly, 50 μl samples or standard were incubated in the wells at 37°C for 30 min and removed, then 50 μl biotinylated detection antibody were added and incubated at 37°C for 30 min. After washing three times, 50 μl horseradish peroxidase conjugate was added and incubated at 37°C for 30 min. After washing five times, the substrate reagent was added and incubated at 37°C for 15 min in the dark, then the absorbance at 450 nm was measured by a microplate reader (Multiskan™ FC, ThermoFisher, MA, USA).

CCK-8 assay

Cells were seeded 3,000/well in 96-well plates, 3 replicates per group. At 24 h, 48 h, 72 h and 96 h after seeding, CCK-8 solution (Sigma-Aldrich, USA) was added to each well and incubation at 37°C for 1 h, then the OD value at 450 nm was measured by using a microplate reader (BIO-RAD, USA), and the cell growth curve was plotted.

Colony formation assay

Cells were seeded 500 cells per well in 6-well plates. After 7-14 days, the surviving cancer cells were washed with cold PBS, fixed with 4% Polyoxymethylene and stained with 0.1% crys-

tal violet, then count the number of clones containing more than 50 cells under the microscope and take photos.

PI staining

T98G and U251MG cells were seeded 5×10^5 cells/well in 6-well Plates, then treated with 0.02% DMSO, 0.1 nM Staurosporine, 0.1 μM Rapamycin, 0.1 μM Nigericin or 10 μM Erastin. After 48 hours of stimulation, cells were harvested and stained with 1 ng/ml propidium iodide (PI), then validated by flow cytometry using a CytoFLEX LX. PI positive cells were calculated as death cells. All experiments were analyzed in triplicates.

IC_{50} calculation

The IC_{50} values of ferroptosis inducers Erastin and RSL3 in GBM cell lines were determined using the CCK-8 solution (Sigma-Aldrich, USA). GBM cells were seeded 3,000/well in 96-well plates and treated with DMSO, gradient dilutions of Erastin (MCE, HY-15763) or RSL3 (MCE, HY-100218A) for 48 h. After treatment, CCK-8 solution (1:10 dilution in medium) was added to each well, and the plate was incubated at 37°C for 2 h. The OD450 of each well was measured using a Multiskan GO (Thermo Fisher). The percentage of cell viability was calculated by mean OD treatment/mean OD control×100, and IC50 was calculated using GraphPad Prism 9.0 software (GraphPad Software, San Diego, CA, USA). A four-parameter logistic regression model was fitted to the dose-response curve (cell viability percentage vs. log10 of drug concentration) to generate the IC_{50} value, with 95% confidence intervals (CIs) reported. Each experiment was independently repeated at least three times to ensure reproducibility of the results.

BODIPY-C11 staining for lipid peroxidation analysis

Lipid peroxidation was assessed using the Lipid Peroxidation Assay Kit with BODIPY 581/591 C11 (Beyotime Biotechnology, S0043S). Cells were seeded 2×10^5/well in six-well plates, then treated with 0.02% DMSO or Erastin (2 μM) or RSL3 (1 μM) for 12 h. Cells were suspended in 1 ml of PBS containing 2 mM BODIPYTM 581/591 C11. The suspension was then incubated for 20 min at 37°C in a tissue culture incubator. After incubation, the cells were washed and resuspended in 300 μl of fresh PBS. Subsequently, the stained cells were immediately analyzed using a flow cytometer (Beckman Cytoflex LS), the ratio of the mean fluorescence intensity (MFI) of oxidized C11 (FITC channel) was calculated for each sample. To account for variations, the data were normalized to control samples, as indicated by relative lipid ROS levels.

RNA-seq and analysis

Total RNA was extracted with a VeZol-Pure Total RNA Isolation Kit (Vazyme, RC202-01) and subjected to RNA-seq on an Illumina platform in PE150 mode by Berry Genomics Co., Ltd. Transcriptome sequencing data were adapter-trimmed using fastp, aligned to the hg38 reference genome with Bowtie, and quantified using RSEM. Differential expression analysis was performed with the R package DESeq2, with an adjusted *p*-value threshold set at < 0.05. Volcano plots were generated using the R packages enhancedVolcano, and GSEA was conducted using GSEA 4.1.0.

Quantification and statistical analysis

Statistical analysis was performed using RStudio or GraphPad Prism 9.0.0 software. All data are presented as the mean ± standard error from three or more independent experiments. Student's *t*-test (2-tailed unpaired) is used to compare two groups, one-way ANOVA followed by multiple comparisons testing is used to compare the means of three or more groups, a *p*-value less than 0.05 was considered statistically significant.

Acknowledgements

We appreciate the technical support of the Center for Scientific Research in the School of Life Sciences, Anhui Medical University. This work was supported by a grant from the National Natural Science Foundation of China project (82073256), a grant from Anhui Provincial Natural Science Foundation (25080-85MH210), a talent start-up program and a research and innovation talent team from Anhui Medical University.

Disclosure of conflict of interest

None.

Address correspondence to: Dr. Mafei Xu and Lu Zhang, Department of Cell Biology, School of Life Sciences, Anhui Medical University, Hefei 230032,

Anhui, China. E-mail: xumafei@ahmu.edu.cn (MFX); zhanglu2323@ahmu.edu.cn (LZ)

References

[1] Weller M, Wen PY, Chang SM, Dirven L, Lim M, Monje M and Reifenberger G. Glioma. Nat Rev Dis Primers 2024; 10: 33.

[2] Louis DN, Perry A, Wesseling P, Brat DJ, Cree IA, Figarella-Branger D, Hawkins C, Ng HK, Pfister SM, Reifenberger G, Soffietti R, von Deimling A and Ellison DW. The 2021 WHO classification of tumors of the central nervous system: a summary. Neuro Oncol 2021; 23: 1231-1251.

[3] Ma X, Sun C, Ding X, Xu J, Zhang Y, Deng T, Wang Y, Yang H, Ding R, Li H, Wang D and Zheng M. Mechanism analysis and targeted therapy of IDH gene mutation in glioma. Am J Cancer Res 2025; 15: 248-270.

[4] Yan H, Parsons DW, Jin G, McLendon R, Rasheed BA, Yuan W, Kos I, Batinic-Haberle I, Jones S, Riggins GJ, Friedman H, Friedman A, Reardon D, Herndon J, Kinzler KW, Velculescu VE, Vogelstein B and Bigner DD. IDH1 and IDH2 mutations in gliomas. N Engl J Med 2009; 360: 765-773.

[5] Han S, Liu Y, Cai SJ, Qian M, Ding J, Larion M, Gilbert MR and Yang C. IDH mutation in glioma: molecular mechanisms and potential therapeutic targets. Br J Cancer 2020; 122: 1580-1589.

[6] Parsons DW, Jones S, Zhang X, Lin JC, Leary RJ, Angenendt P, Mankoo P, Carter H, Siu IM, Gallia GL, Olivi A, McLendon R, Rasheed BA, Keir S, Nikolskaya T, Nikolsky Y, Busam DA, Tekleab H, Diaz LA Jr, Hartigan J, Smith DR, Strausberg RL, Marie SK, Shinjo SM, Yan H, Riggins GJ, Bigner DD, Karchin R, Papadopoulos N, Parmigiani G, Vogelstein B, Velculescu VE and Kinzler KW. An integrated genomic analysis of human glioblastoma multiforme. Science 2008; 321: 1807-1812.

[7] Xu W, Yang H, Liu Y, Yang Y, Wang P, Kim SH, Ito S, Yang C, Wang P, Xiao MT, Liu LX, Jiang WQ, Liu J, Zhang JY, Wang B, Frye S, Zhang Y, Xu YH, Lei QY, Guan KL, Zhao SM and Xiong Y. Oncometabolite 2-hydroxyglutarate is a competitive inhibitor of alpha-ketoglutarate-dependent dioxygenases. Cancer Cell 2011; 19: 17-30.

[8] Chowdhury R, Yeoh KK, Tian YM, Hillringhaus L, Bagg EA, Rose NR, Leung IK, Li XS, Woon EC, Yang M, McDonough MA, King ON, Clifton IJ, Klose RJ, Claridge TD, Ratcliffe PJ, Schofield CJ and Kawamura A. The oncometabolite 2-hydroxyglutarate inhibits histone lysine demethylases. EMBO Rep 2011; 12: 463-469.

[9] Gunn K, Myllykoski M, Cao JZ, Ahmed M, Huang B, Rouaisnel B, Diplas BH, Levitt MM, Looper R, Doench JG, Ligon KL, Kornblum HI, McBrayer SK, Yan H, Duy C, Godley LA, Koivunen P and Losman JA. (R)-2-Hydroxyglutarate inhibits KDM5 histone lysine demethylases to drive transformation in IDH-mutant cancers. Cancer Discov 2023; 13: 1478-1497.

[10] Dang L, White DW, Gross S, Bennett BD, Bittinger MA, Driggers EM, Fantin VR, Jang HG, Jin S, Keenan MC, Marks KM, Prins RM, Ward PS, Yen KE, Liau LM, Rabinowitz JD, Cantley LC, Thompson CB, Vander Heiden MG and Su SM. Cancer-associated IDH1 mutations produce 2-hydroxyglutarate. Nature 2009; 462: 739-744.

[11] Ward PS, Patel J, Wise DR, Abdel-Wahab O, Bennett BD, Coller HA, Cross JR, Fantin VR, Hedvat CV, Perl AE, Rabinowitz JD, Carroll M, Su SM, Sharp KA, Levine RL and Thompson CB. The common feature of leukemia-associated IDH1 and IDH2 mutations is a neomorphic enzyme activity converting alpha-ketoglutarate to 2-hydroxyglutarate. Cancer Cell 2010; 17: 225-234.

[12] Noushmehr H, Weisenberger DJ, Diefes K, Phillips HS, Pujara K, Berman BP, Pan F, Pelloski CE, Sulman EP, Bhat KP, Verhaak RG, Hoadley KA, Hayes DN, Perou CM, Schmidt HK, Ding L, Wilson RK, Van Den Berg D, Shen H, Bengtsson H, Neuvial P, Cope LM, Buckley J, Herman JG, Baylin SB, Laird PW and Aldape K; Cancer Genome Atlas Research Network. Identification of a CpG island methylator phenotype that defines a distinct subgroup of glioma. Cancer Cell 2010; 17: 510-522.

[13] Turcan S, Rohle D, Goenka A, Walsh LA, Fang F, Yilmaz E, Campos C, Fabius AW, Lu C, Ward PS, Thompson CB, Kaufman A, Guryanova O, Levine R, Heguy A, Viale A, Morris LG, Huse JT, Mellinghoff IK and Chan TA. IDH1 mutation is sufficient to establish the glioma hypermethylator phenotype. Nature 2012; 483: 479-483.

[14] Zhang L, He L, Lugano R, Roodakker K, Bergqvist M, Smits A and Dimberg A. IDH mutation status is associated with distinct vascular gene expression signatures in lower-grade gliomas. Neuro Oncol 2018; 20: 1505-1516.

[15] Wu MJ, Kondo H, Kammula AV, Shi L, Xiao Y, Dhiab S, Xu Q, Slater CJ, Avila OI, Merritt J, Kato H, Kattel P, Sussman J, Gritti I, Eccleston J, Sun Y, Cho HM, Olander K, Katsuda T, Shi DD, Savani MR, Smith BC, Cleary JM, Mostoslavsky R, Vijay V, Kitagawa Y, Wakimoto H, Jenkins RW, Yates KB, Paik J, Tassinari A, Saatcioglu DH, Tron AE, Haas W, Cahill D, McBrayer SK, Manguso RT and Bardeesy N. Mutant IDH1 inhibition induces dsDNA sensing to activate tumor immunity. Science 2024; 385: eadl6173.

[16] Aguilera P and Lopez-Contreras AJ. ATRX, a guardian of chromatin. Trends Genet 2023; 39: 505-519.

[17] Schwartzentruber J, Korshunov A, Liu XY, Jones DT, Pfaff E, Jacob K, Sturm D, Fontebasso AM, Quang DA, Tonjes M, Hovestadt V, Albrecht S, Kool M, Nantel A, Konermann C, Lindroth A, Jager N, Rausch T, Ryzhova M, Korbel JO, Hielscher T, Hauser P, Garami M, Klekner A, Bognar L, Ebinger M, Schuhmann MU, Scheurlen W, Pekrun A, Fruhwald MC, Roggendorf W, Kramm C, Durken M, Atkinson J, Lepage P, Montpetit A, Zakrzewska M, Zakrzewski K, Liberski PP, Dong Z, Siegel P, Kulozik AE, Zapatka M, Guha A, Malkin D, Felsberg J, Reifenberger G, von Deimling A, Ichimura K, Collins VP, Witt H, Milde T, Witt O, Zhang C, Castelo-Branco P, Lichter P, Faury D, Tabori U, Plass C, Majewski J, Pfister SM and Jabado N. Driver mutations in histone H3.3 and chromatin remodelling genes in paediatric glioblastoma. Nature 2012; 482: 226-231.

[18] Cancer Genome Atlas Research Network; Brat DJ, Verhaak RG, Aldape KD, Yung WK, Salama SR, Cooper LA, Rheinbay E, Miller CR, Vitucci M, Morozova O, Robertson AG, Noushmehr H, Laird PW, Cherniack AD, Akbani R, Huse JT, Ciriello G, Poisson LM, Barnholtz-Sloan JS, Berger MS, Brennan C, Colen RR, Colman H, Flanders AE, Giannini C, Grifford M, Iavarone A, Jain R, Joseph I, Kim J, Kasaian K, Mikkelsen T, Murray BA, O'Neill BP, Pachter L, Parsons DW, Sougnez C, Sulman EP, Vandenberg SR, Van Meir EG, von Deimling A, Zhang H, Crain D, Lau K, Mallery D, Morris S, Paulauskis J, Penny R, Shelton T, Sherman M, Yena P, Black A, Bowen J, Dicostanzo K, Gastier-Foster J, Leraas KM, Lichtenberg TM, Pierson CR, Ramirez NC, Taylor C, Weaver S, Wise L, Zmuda E, Davidsen T, Demchok JA, Eley G, Ferguson ML, Hutter CM, Mills Shaw KR, Ozenberger BA, Sheth M, Sofia HJ, Tarnuzzer R, Wang Z, Yang L, Zenklusen JC, Ayala B, Baboud J, Chudamani S, Jensen MA, Liu J, Pihl T, Raman R, Wan Y, Wu Y, Ally A, Auman JT, Balasundaram M, Balu S, Baylin SB, Beroukhim R, Bootwalla MS, Bowlby R, Bristow CA, Brooks D, Butterfield Y, Carlsen R, Carter S, Chin L, Chu A, Chuah E, Cibulskis K, Clarke A, Coetzee SG, Dhalla N, Fennell T, Fisher S, Gabriel S, Getz G, Gibbs R, Guin R, Hadjipanayis A, Hayes DN, Hinoue T, Hoadley K, Holt RA, Hoyle AP, Jefferys SR, Jones S, Jones CD, Kucherlapati R, Lai PH, Lander E, Lee S, Lichtenstein L, Ma Y, Maglinte DT, Mahadeshwar HS, Marra MA, Mayo M, Meng S, Meyerson ML, Mieczkowski PA, Moore RA, Mose LE, Mungall AJ, Pantazi A, Parfenov M, Park PJ, Parker JS, Perou CM, Protopopov A, Ren X, Roach J, Sabedot TS, Schein J, Schumacher SE, Seidman JG, Seth S, Shen H, Simons JV, Sipahimalani P, Soloway MG, Song X, Sun H, Tabak B, Tam A, Tan D, Tang J, Thiessen N, Triche T Jr, Van Den Berg DJ, Veluvolu U, Waring S, Weisenberger DJ, Wilkerson MD, Wong T, Wu J, Xi L, Xu AW, Yang L, Zack TI, Zhang J, Aksoy BA, Arachchi H, Benz C, Bernard B, Carlin D, Cho J, DiCara D, Frazer S, Fuller GN, Gao J, Gehlenborg N, Haussler D, Heiman DI, Iype L, Jacobsen A, Ju Z, Katzman S, Kim H, Knijnenburg T, Kreisberg RB, Lawrence MS, Lee W, Leinonen K, Lin P, Ling S, Liu W, Liu Y, Liu Y, Lu Y, Mills G, Ng S, Noble MS, Paull E, Rao A, Reynolds S, Saksena G, Sanborn Z, Sander C, Schultz N, Senbabaoglu Y, Shen R, Shmulevich I, Sinha R, Stuart J, Sumer SO, Sun Y, Tasman N, Taylor BS, Voet D, Weinhold N, Weinstein JN, Yang D, Yoshihara K, Zheng S, Zhang W, Zou L, Abel T, Sadeghi S, Cohen ML, Eschbacher J, Hattab EM, Raghunathan A, Schniederjan MJ, Aziz D, Barnett G, Barrett W, Bigner DD, Boice L, Brewer C, Calatozzolo C, Campos B, Carlotti CG Jr, Chan TA, Cuppini L, Curley E, Cuzzubbo S, Devine K, DiMeco F, Duell R, Elder JB, Fehrenbach A, Finocchiaro G, Friedman W, Fulop J, Gardner J, Hermes B, Herold-Mende C, Jungk C, Kendler A, Lehman NL, Lipp E, Liu O, Mandt R, McGraw M, McLendon R, McPherson C, Neder L, Nguyen P, Noss A, Nunziata R, Ostrom QT, Palmer C, Perin A, Pollo B, Potapov A, Potapova O, Rathmell WK, Rotin D, Scarpace L, Schilero C, Senecal K, Shimmel K, Shurkhay V, Sifri S, Singh R, Sloan AE, Smolenski K, Staugaitis SM, Steele R, Thorne L, Tirapelli DP, Unterberg A, Vallurupalli M, Wang Y, Warnick R, Williams F, Wolinsky Y, Bell S, Rosenberg M, Stewart C, Huang F, Grimsby JL, Radenbaugh AJ and Zhang J. Comprehensive, integrative genomic analysis of diffuse lower-grade gliomas. N Engl J Med 2015; 372: 2481-2498.

[19] Heaphy CM, de Wilde RF, Jiao Y, Klein AP, Edil BH, Shi C, Bettegowda C, Rodriguez FJ, Eberhart CG, Hebbar S, Offerhaus GJ, McLendon R, Rasheed BA, He Y, Yan H, Bigner DD, Oba-Shinjo SM, Marie SK, Riggins GJ, Kinzler KW, Vogelstein B, Hruban RH, Maitra A, Papadopoulos N and Meeker AK. Altered telomeres in tumors with ATRX and DAXX mutations. Science 2011; 333: 425.

[20] Mukherjee J, Johannessen TC, Ohba S, Chow TT, Jones L, Pandita A and Pieper RO. Mutant IDH1 cooperates with ATRX loss to drive the alternative lengthening of telomere phenotype in glioma. Cancer Res 2018; 78: 2966-2977.

[21] Hariharan S, Whitfield BT, Pirozzi CJ, Waitkus MS, Brown MC, Bowie ML, Irvin DM, Roso K, Fuller R, Hostettler J, Dharmaiah S, Gibson EA, Briley A, Mangoli A, Fraley C, Shobande M, Stevenson K, Zhang G, Malgulwar PB, Roberts H, Roskoski M, Spasojevic I, Keir ST, He Y, Castro MG, Huse JT and Ashley DM. Interplay between ATRX and IDH1 mutations governs in-

nate immune responses in diffuse gliomas. Nat Commun 2024; 15: 730.
[22] Jiang X, Stockwell BR and Conrad M. Ferroptosis: mechanisms, biology and role in disease. Nat Rev Mol Cell Biol 2021; 22: 266-282.
[23] Ni R, Jiang J, Wang F and Min J. Treating incurable non-communicable diseases by targeting iron metabolism and ferroptosis. Sci China Life Sci 2025; 68: 2243-2263.
[24] Yang WS, SriRamaratnam R, Welsch ME, Shimada K, Skouta R, Viswanathan VS, Cheah JH, Clemons PA, Shamji AF, Clish CB, Brown LM, Girotti AW, Cornish VW, Schreiber SL and Stockwell BR. Regulation of ferroptotic cancer cell death by GPX4. Cell 2014; 156: 317-331.
[25] Seiler A, Schneider M, Forster H, Roth S, Wirth EK, Culmsee C, Plesnila N, Kremmer E, Radmark O, Wurst W, Bornkamm GW, Schweizer U and Conrad M. Glutathione peroxidase 4 senses and translates oxidative stress into 12/15-lipoxygenase dependent- and AIF-mediated cell death. Cell Metab 2008; 8: 237-248.
[26] Dixon SJ, Patel DN, Welsch M, Skouta R, Lee ED, Hayano M, Thomas AG, Gleason CE, Tatonetti NP, Slusher BS and Stockwell BR. Pharmacological inhibition of cystine-glutamate exchange induces endoplasmic reticulum stress and ferroptosis. Elife 2014; 3: e02523.
[27] Sun J, Yang J, Tao J, Yang Y, Wang R, Zhang H, Liu W, Zhao S, Shao R, He Y, Tao S, Li Y, Qu H, Liu D, Li J, Jiang J, Deng B, Gao C, Lin P, Zeng L, Meng P and Wang G. Delaying pyroptosis with an AI-screened gasdermin D pore blocker mitigates inflammatory response. Nat Immunol 2025; 26: 1660-1672.
[28] Chae HJ, Kang JS, Byun JO, Han KS, Kim DU, Oh SM, Kim HM, Chae SW and Kim HR. Molecular mechanism of staurosporine-induced apoptosis in osteoblasts. Pharmacol Res 2000; 42: 373-381.
[29] Saxton RA and Sabatini DM. mTOR signaling in growth, metabolism, and disease. Cell 2017; 168: 960-976.
[30] Johnson BE, Mazor T, Hong C, Barnes M, Aihara K, McLean CY, Fouse SD, Yamamoto S, Ueda H, Tatsuno K, Asthana S, Jalbert LE, Nelson SJ, Bollen AW, Gustafson WC, Charron E, Weiss WA, Smirnov IV, Song JS, Olshen AB, Cha S, Zhao Y, Moore RA, Mungall AJ, Jones SJM, Hirst M, Marra MA, Saito N, Aburatani H, Mukasa A, Berger MS, Chang SM, Taylor BS and Costello JF. Mutational analysis reveals the origin and therapy-driven evolution of recurrent glioma. Science 2014; 343: 189-193.
[31] Philip B, Yu DX, Silvis MR, Shin CH, Robinson JP, Robinson GL, Welker AE, Angel SN, Tripp SR, Sonnen JA, VanBrocklin MW, Gibbons RJ, Looper RE, Colman H and Holmen SL. Mutant IDH1 promotes glioma formation in vivo. Cell Rep 2018; 23: 1553-1564.
[32] Miller JJ and Cahill DP. MGMT promoter methylation and hypermutant recurrence in IDH mutant lower-grade glioma. Neuro Oncol 2020; 22: 1553-1554.
[33] Kohanbash G, Carrera DA, Shrivastav S, Ahn BJ, Jahan N, Mazor T, Chheda ZS, Downey KM, Watchmaker PB, Beppler C, Warta R, Amankulor NA, Herold-Mende C, Costello JF and Okada H. Isocitrate dehydrogenase mutations suppress STAT1 and CD8+ T cell accumulation in gliomas. J Clin Invest 2017; 127: 1425-1437.
[34] Hu C, Wang K, Damon C, Fu Y, Ma T, Kratz L, Lal B, Ying M, Xia S, Cahill DP, Jackson CM, Lim M, Laterra J and Li Y. ATRX loss promotes immunosuppressive mechanisms in IDH1 mutant glioma. Neuro Oncol 2022; 24: 888-900.
[35] Hassannia B, Vandenabeele P and Vanden Berghe T. Targeting ferroptosis to iron out cancer. Cancer Cell 2019; 35: 830-849.
[36] Gan B. ACSL4, PUFA, and ferroptosis: new arsenal in anti-tumor immunity. Signal Transduct Target Ther 2022; 7: 128.
[37] Hoadley KA, Yau C, Hinoue T, Wolf DM, Lazar AJ, Drill E, Shen R, Taylor AM, Cherniack AD, Thorsson V, Akbani R, Bowlby R, Wong CK, Wiznerowicz M, Sanchez-Vega F, Robertson AG, Schneider BG, Lawrence MS, Noushmehr H, Malta TM; Cancer Genome Atlas Network; Stuart JM, Benz CC and Laird PW. Cell-of-origin patterns dominate the molecular classification of 10,000 tumors from 33 types of cancer. Cell 2018; 173: 291-304, e6.
[38] Gerhauser C, Favero F, Risch T, Simon R, Feuerbach L, Assenov Y, Heckmann D, Sidiropoulos N, Waszak SM, Hubschmann D, Urbanucci A, Girma EG, Kuryshev V, Klimczak LJ, Saini N, Stutz AM, Weichenhan D, Bottcher LM, Toth R, Hendriksen JD, Koop C, Lutsik P, Matzk S, Warnatz HJ, Amstislavskiy V, Feuerstein C, Raeder B, Bogatyrova O, Schmitz EM, Hube-Magg C, Kluth M, Huland H, Graefen M, Lawerenz C, Henry GH, Yamaguchi TN, Malewska A, Meiners J, Schilling D, Reisinger E, Eils R, Schlesner M, Strand DW, Bristow RG, Boutros PC, von Kalle C, Gordenin D, Sultmann H, Brors B, Sauter G, Plass C, Yaspo ML, Korbel JO, Schlomm T and Weischenfeldt J. Molecular evolution of early-onset prostate cancer identifies molecular risk markers and clinical trajectories. Cancer Cell 2018; 34: 996-1011, e1018.

Table S1. Antibodies

Antibody Name	Catalog Number	Company Name	Experiment and concentration ratio
Anti-IDH1 Polyclonal antibody	12332-1-AP	Proteintech	WB: 1:1000
Anti-ATRX Polyclonal antibody	ab97508	Abcam	WB: 1:1000
Anti-GAPDH Monoclonal antibody	60004-1-Ig	Proteintech	WB: 1:3000

Table S2. qPCR primers

Primer Name	Sequence (5'-3')	
Human-IDH1	sense	ATGTCCAAAAAAATCAGTGGCG
	antisense	TTAAAGTTTGGCCTGAGCTAGTTTG
Human-ATRX	sense	AGCAATCACAGAAGCCGACA
	antisense	TGCAAGTCGTGGAGGAGAAC
Human-MYC	sense	TACAACACCCGAGCAAGGAC
	antisense	TAACGTTGAGGGGCATCGT
Human-E2F2	sense	AAGGGGAAGTGCATCAGAGTG
	antisense	TCTTGGCCTTCTTGCGGAT
Human-HOMX1	sense	CCAGGCAGAGAATGCTGAGTTC
	antisense	AAGACTGGGCTCTCCTTGTTGC
Human-GPX4	sense	TCACCAAGTTTGGACACCGT
	antisense	ATAGTGGGGCAGGTCCTTCT
Human-SLC7A11	sense	GCCCAAGGGGAGACACAAAA
	antisense	TTGAAGGTTCTTTGCCGTGC
Human-ACSL4	sense	GCTATCTCCTCAGACACACCGA
	antisense	AGGTGCTCCAACTCTGCCAGTA
Human-ACTB	sense	GGCACCCAGCACAATGAAG
	antisense	CCGATCCACACGGAGTACTTG

Table S3. SgRNA oligo sequence

Oligo Name	Sequence (5'-3')	
SgATRX-238	sense	CACCGCAGGATCGTCACGATCAAAG
	antisense	AAACCTTTGATCGTGACGATCCTGC

Table S4. Plasmids

Plasmids Name	Catalog Number	Company Name
pLVX-M-puro	#125839	Addgene
LentiCas9-Blast	#52962	Addgene
LentiGuide-puro	#52963	Addgene

Table S5. Reagents

Reagents Name	Catalog Number	Company Name
Erastin	HY-15763	MedChemExpress
(1S,3R)-RSL3	HY-100218A	MedChemExpress
Staurosporine	HY-15141	MedChemExpress
Rapamycin	HY-10219	MedChemExpress
Nigericin	HY-127019	MedChemExpress

Table S6. Cells

Cells Name	Catalog Number	Company Name
T98G	CRL-1960	American Type Culture Collection
U251MG	CL-0237	Procell system